AIAA 95-1830

Experimental Aerodynamic Characteristics of the Pegasus Air-Launched Booster and Comparisons with Predicted and Flight Results

M. N. Rhode and W. C. Engelund
NASA Langley Research Center
Hampton, VA

M. R. Mendenhall
Nielsen Engineering & Research, Inc.
Mountain View, CA

AIAA 13th Applied Aerodynamics Conference
June 19-22, 1995/San Diego, CA

Experimental Aerodynamic Characteristics of the Pegasus Air-Launched Booster and Comparisons with Predicted and Flight Results

Matthew N. Rhode* and Walter C. Engelund†
NASA Langley Research Center, Hampton, VA 23681
Michael R. Mendenhall‡
Nielsen Engineering & Research, Inc., Mountain View, CA 94043

Experimental longitudinal and lateral-directional aerodynamic characteristics were obtained for the Pegasus and Pegasus XL configurations over a Mach number range from 1.6 to 6 and angles of attack from -4 to +24 degrees. Angle of sideslip was varied from -6 to +6 degrees, and control surfaces were deflected to obtain elevon, aileron, and rudder effectiveness. Experimental data for the Pegasus configuration are compared with engineering code predictions performed by Nielsen Engineering & Research, Inc. (NEAR) in the aerodynamic design of the Pegasus vehicle, and with results from the Aerodynamic Preliminary Analysis System (APAS) code. Comparisons of experimental results are also made with longitudinal flight data from Flight #2 of the Pegasus vehicle. Results show that the longitudinal aerodynamic characteristics of the Pegasus and Pegasus XL configurations are similar, having the same lift-curve slope and drag levels across the Mach number range. Both configurations are longitudinally stable, with stability decreasing towards neutral levels as Mach number increases. Directional stability is negative at moderate to high angles of attack due to separated flow over the vertical tail. Dihedral effect is positive for both configurations, but is reduced 30-50 percent for the Pegasus XL configuration because of the horizontal tail anhedral. Predicted longitudinal characteristics and both longitudinal and lateral-directional control effectiveness are generally in good agreement with experiment. Due to the complex leeside flowfield, lateral-directional characteristics are not as well predicted by the engineering codes. Experiment and flight data are in good agreement across the Mach number range.

Nomenclature

AR	Wing aspect ratio, b^2/S
b	Wing span, in
$\bar{c}$	Reference length, in
C_A	Axial force coefficient, {axial force}$/q_\infty S$
C_D	Drag coefficient, {drag}$/q_\infty S$
C_L	Lift coefficient, {lift}$/q_\infty S$
C_{L_α}	Lift-curve slope, $\partial C_L/\partial\alpha$ at $\alpha = 0^o$
$C_{L_{\delta e}}$	Elevon lift effectiveness, $\Delta C_L/\Delta\delta_e$
C_l	Rolling moment coefficient, {rolling moment}$/q_\infty Sb$
C_{l_β}	Effective dihedral parameter, $\Delta C_L/\Delta\beta$
$C_{l_{\delta a}}$	Aileron roll effectiveness, $\Delta C_l/\Delta\delta_a$
$C_{l_{\delta r}}$	Rudder roll effectiveness, $\Delta C_l/\Delta\delta_r$
C_m	Pitching moment coefficient, {pitching moment}$/q_\infty S\bar{c}$
$C_{m_{\delta e}}$	Elevon pitch effectiveness, $\Delta C_m/\Delta\delta_e$
C_N	Normal force coefficient, {normal force}$/q_\infty S$
C_n	Yawing moment coefficient, {yawing moment}$/q_\infty Sb$
C_{n_β}	Directional stability parameter, $\Delta C_n/\Delta\beta$
$C_{n_{\delta a}}$	Aileron yaw effectiveness, $\Delta C_n/\Delta\delta_a$
$C_{n_{\delta r}}$	Rudder yaw effectiveness, $\Delta C_n/\Delta\delta_r$
C_Y	Side force coefficient, {side force}$/q_\infty S$
C_{Y_β}	Side force parameter, $\Delta C_Y/\beta$
L	Model length, in

*Aerospace Technologist, Aerothermodynamics Branch, Gas Dynamics Division. Member AIAA.
†Aerospace Technologist, Vehicle Analysis Branch, Space Systems and Concepts Division. Member AIAA.
‡Vice President. AIAA Associate Fellow.

L/D	Lift-to-drag ratio
M	Mach number
p	Pressure, lb/in^2
q	Dynamic pressure, lb/in^2
Re	Unit Reynolds number, 1/ft
S	Reference area, in^2
T	Temperature, °R
X	Longitudinal model body axis
Y	Lateral model body axis
Z	Vertical model body axis
α	Angle of attack, deg
β	Angle of sideslip, deg
δ_a	Aileron deflection angle, $\delta_{e,l} - \delta_{e,r}$, deg
δ_e	Elevon deflection angle, $(\delta_{e,l} + \delta_{e,r})/2$, deg
δ_r	Rudder deflection angle, deg
Γ_{tail}	Horizontal tail dihedral angle, deg
Λ_{LE}	Wing leading edge sweep angle, deg
λ	Wing taper ratio

Subscripts:

cp	Center of pressure
max	Maximum
t	Reservior conditions
0	Zero-lift
∞	Freestream static conditions

Introduction

With the growing emergence of micro-satellites in the commercial launch market, there has been increasing interest in small-payload-to-orbit vehicles (SPOV) capable of delivering 1000–2000 lb payloads to LEO at reduced cost.[1] Several concepts for SPOVs have emerged, including both expendable and partially reusable vehicles, launched from the ground or air-launched from a carrier aircraft. The latter concept is receiving considerable attention due to the many advantages of airborne launch. For example, booster performance is enhanced by the kinetic energy imparted by the carrier aircraft, and structural weight can be reduced due to the lower dynamic pressures and resulting reduced structural stresses encountered at launch altitude.[2] Additionally, airborne launch allows the ability to launch into any orbital inclination or into trajectories suitable for a variety of hypersonic testbed missions.[3,4] In the current X-34 program to develop a small demonstration launch vehicle, an air-launched configuration was chosen from several concepts.[5]

The viability of an air-launched booster concept has been demonstrated with the Pegasus vehicle. Pegasus is a three-stage, solid-rocket-propelled, winged booster capable of delivering 900 lb of payload to LEO. Developed jointly by Orbital Sciences Corporation (OSC) and Hercules Aerospace Company, Pegasus first flew in April, 1991, and has since flown several missions. The vehicle is carried aloft by a B-52 carrier aircraft and dropped at a prescribed altitude and velocity. A photograph of the Pegasus/B-52 launch system is shown in Figure 1. Recently, OSC has developed the Pegasus XL vehicle, a lengthened version of Pegasus with increased performance and payload capacity, designed to launch from a L-1011 aircraft.

The Pegasus vehicle was designed solely using engineering codes, supported by limited computational fluid dynamic (CFD) predictions, thus without the benefit of wind tunnel data.[6,7] To tie in experimental ground test data with existing predictions and flight test results, a series of wind tunnel tests were performed by the Aerothermodynamics Branch of the NASA Langley Research Center on the Pegasus, and later, Pegasus XL configurations. The synergistic combination of wind tunnel, computational, and flight results will provide a comprehensive database for calibration and improvement of the analytical tools that will be used in the design of future air-launched SPOVs.

Three-percent-scale models of the Pegasus and Pegasus XL configurations were tested in the NASA Langley Research Center Unitary Plan Wind Tunnel (UPWT) and the 20-Inch Mach 6 Tunnel to obtain longitudinal and lateral/directional aerodynamic characteristics over a Mach number range from 1.6 to 6. This paper presents some results of that experimental study, showing effects of Mach number, attitude, and control surface deflection on the aerodynamic performance, stability, control, and trim characteristics of the Pegasus and Pegasus XL configuration. Also presented are comparisons of the experimental results with predictions from the Langley Aerodynamic Preliminary Analysis System (APAS) and engineering codes used by Nielsen Engineering and Research, Inc. (NEAR) in the design of the Pegasus vehicle, and with flight data.

Experimental Method

Models

Tests were performed using 3-percent-scale, machined, stainless-steel models of the Pegasus and Pegasus XL configurations. Sketches and photographs of the models are shown in Figures 2 through 4. The Pegasus configuration has a cylindrical fuselage with a blunt nose. A clipped delta wing is mounted on a large fillet on top of the fuselage. Inboard, the wing has a double-wedge airfoil section, transitioning to a diamond section towards the wing tip. The all-moveable horizontal and vertical tails are identical in size and shape. On the model, the tail surfaces can be deflected ±20 degrees in 5-degree increments. Raceways fore and aft of the wing/fuselage fillet are removable and can be replaced

with flush inserts. The model is sting-mounted through the base, with the inside base surface contoured to simulate the rocket nozzle. The sting was affixed to the tunnel support mechanism more than ten sting diameters downstream of the model base to minimize support interference effects. The triangular flat region on the upper surface of the wing was used to level the model in both pitch and roll.

The Pegasus XL model is formed by replacing forward and aft sections of the model to lengthen the fuselage and place the horizontal tails at an anhedral angle of 23 degrees. The middle fuselage section, wing, and tail surfaces are common to both models. A summary of dimensional information for both models is found in Table 1.

Facilities

The Langley UPWT is a supersonic closed-circuit pressure tunnel with two test legs. The flow in the low-speed leg (Test Section #1) can be varied from a Mach number of 1.5 to 2.86. The high-speed leg (Test Section #2) produces flow Mach numbers from 2.36 to 4.63. Both legs have test sections of $4 \times 4 \times 7$ feet in size and utilize two-dimensional, asymmetric sliding-block type nozzles to provide continuous variation in Mach number. The model support mechanisms allow remote control of angle of attack, sideslip, and roll, as well as axial position in the test sections. A more complete description of this facility can be found in Reference 8.

The Langley 20-Inch Mach 6 Tunnel is a blowdown wind tunnel utilizing dry air as the test gas. The air is heated to a maximum temperature of 1000°R using an electrical resistance heater, with a maximum reservoir pressure of 525 psia, before expanding through a fixed, two-dimensional, contoured nozzle into a 20-inch-square test section. An injection system is used to move the model into the flow from a sheltered position following tunnel start and establishment of the desired flow conditions. This injection process is required to protect the model and strain-gauge balance from tunnel start-up loads and to minimize heating to the balance. Run times are typically from 2 to 10 minutes depending on the reservoir pressure and vacuum levels. This facility is discussed in more detail in Reference 9.

Test Conditions

For the present investigation, tests were performed in the low-speed leg of the UPWT at Mach numbers of 1.60 and 2.00, and in the high-speed leg at Mach numbers of 2.50, 2.96, 3.95, and 4.63. In both legs, the freestream unit Reynolds number at all Mach numbers was maintained at 2×10^6 per foot. Flow conditions were determined from reservoir conditions and the current calibration of the tunnel. In the UPWT, angle of attack was varied in a pitch-pause mode from -4 degrees to a maximum of 20 degrees for the Pegasus model and 24 degrees for the Pegasus XL model at angles of sideslip of 0 and 2 degrees. Angle of sideslip was varied from -6 to $+6$ degrees at fixed angles of attack. An attempt was made to keep the model angle of attack range close to the flight vehicle trajectory to limit the test matrix, thereby shortening tunnel occupancy time.

In the 20-Inch Mach 6 Tunnel, runs were performed over a range of freestream unit Reynolds number from 1×10^6 per foot to 3×10^6 per foot. Flow conditions were determined from reservoir conditions and the stagnation pressure measured via a pitot probe in the test section. Angle of attack was varied in a pitch-pause mode from -2 to +8 degrees at angles of sideslip of 0 and 2 degrees. At fixed angles of attack, angle of sideslip was varied from -3 to +3 degrees.

A summary of flow conditions for both facilities may be found in Table 2.

Instrumentation and Setup

Aerodynamic forces and moments acting on the model were measured with internally-mounted, six-component, strain-gauge balances affixed to a straight sting. The balance used in the 20-Inch Mach 6 Tunnel was water-cooled to minimize measurement errors induced by thermal stresses. Pressure transducers external to the model were used to measure chamber pressure in the balance cavity by way of thin tubing routed up the sides of the sting. An electrical fouling strip was placed on the sting at the model exit to signal any fouling on the model support.

At supersonic conditions, transition strips were applied to the forebody nose and leading edges of the wing and tail surfaces to ensure boundary-layer transition to turbulent flow.[10] For Mach numbers of 1.60 and 2.00, No. 60 sand was sprinkled in a 1/8-inch-wide strip, 1.2 inches streamwise from the stagnation point on the nose, and 0.4 inches streamwise from the wing and tail surface leading edges. At the higher Mach numbers, individual grains of No. 35 grit were placed in the same positions relative to the nose and leading edges. Grit spacing was dependent on the local leading edge sweep angle, hence varying among the nose, wing, and tail surfaces. No attempt was made to trip the flow in the 20-Inch Mach 6 Tunnel.

Data Reduction and Uncertainty

Conventions for the coordinate system, forces, moments, and attitude angles are shown in Figure 5. The force and moment data were reduced to coefficient form using the reference dimensions given in Table 1 and a moment reference center of approximately 59 percent of the body length for the Pegasus model and 58 percent

for the Pegasus XL model. The coefficient data are corrected for chamber pressure in the model, and angles of attack and sideslip are corrected for flow angularity and deflections of the sting and balance under aerodynamic load. Lateral-directional derivatives were calculated from body-axis data at fixed angles of sideslip of 0 and 2 degrees.

Estimated uncertainties in the static aerodynamic coefficients are given in Table 3 for the various test Mach numbers. For the 20-Inch Mach 6 Tunnel, the listed uncertainties are for a condition corresponding to a unit Reynolds number of 2×10^6 per foot. The uncertainty analysis was based on the method of propagation of errors and took into account uncertainty in the strain-gauge balance measurements; uncertainty in angles of attack and sideslip; and uncertainty in dynamic pressure.[11-13] Balance measurement uncertainties were based on statistically-derived values from the hundreds of loadings performed during the balance calibration.[14] Uncertainty in angles of attack and sideslip was estimated to be 0.10 degrees, including sting/balance deflection and flow angularity. While the uncertainty in the measurement of dynamic pressure is very small, the variation in dynamic pressure across the test sections of the two facilities is approximately 2 percent. Repeat points taken at the end of every pitch sweep and from separate runs show the data repeatability to be within the uncertainties given in Table 3.

Flow Visualization

Flow visualization data in the form of schlieren and vapor screen photographs were obtained in the UPWT. Shock wave patterns were observed using a single-pass schlieren system with the knife edge in a horizontal orientation. The vapor screen photographs were taken with a still camera mounted inside the tunnel and above and behind the model. Water vapor was introduced into the flow, and a laser light sheet was projected across the test section to illuminate a cross section of the flowfield. The model was traversed through the light sheet to observe the flowfield at various model stations. In the vapor screen photographs, the envelopes of the shock waves are seen as light-colored regions. Dark-colored regions denote low-pressure zones, such as vortices. Schlieren and oil-flow photographs were obtained in the 20-Inch Mach 6 Tunnel, but are not presented here.

Prediction Methods

APAS

The Aerodynamic Preliminary Analysis System, or APAS, is an interactive computer program that was developed to estimate the aerodynamic characteristics of aerospace vehicles.[15] As the name implies, its intent is a preliminary evaluation tool used to obtain quick estimations of configuration aerodynamics, including longitudinal and lateral-directional static, dynamic, and control effectiveness characteristics of arbitrary three-dimensional configurations throughout the speed regime.

In the subsonic and low supersonic speed regimes, APAS utilizes a combination of slender body theory, linearized chordplane source and vortex panel distributions, and empirical viscous and wave drag estimation techniques. In the supersonic through hypersonic flight regime a non-interference finite element model of the vehicle is analyzed using a variety of theoretical and empirical impact pressure methods along with various approximate boundary layer relations.[16] The supersonic/hypersonic analysis module used in APAS is essentially an enhanced version of the Hypersonic Arbitrary Body Program Mark III (HABP).[17] In this particular study, all of the APAS solutions at Mach numbers below three were computed using the slender body/linear panel code methods. At higher Mach numbers, the hypersonic impact methods were used. All of the APAS solutions included in this study were computed for wind tunnel conditions.

NEAR Aerodynamic Predictions

The NEAR predictions were performed using a variety of engineering codes and panel methods.[5] At Mach numbers below 4.0, MISL3 and Missile DATCOM were used in parallel to predict longitudinal and lateral-directional aerodynamics. These independent codes employ a combination of theoretical methods and empirical databases which inherently account for viscous effects, non-linear high-angle-of-attack aerodynamics, and control surface interference. At higher Mach numbers, impact method codes such as S/HABP and MADM were used for aerodynamic predictions. Subsonic and supersonic panel method codes were used for aerodynamic calculations, particularly at high angles of attack where forebody vortex effects had to be included. The aerodynamic database was assembled based on experience of the individual strengths and weaknesses of each code. Higher-order methods such as Euler and Navier-Stokes solutions were used to check important points on the trajectory. The results from the NEAR predictions included in this paper were all computed prior to the wind tunnel tests at flight conditions based on a nominal flight trajectory.

Flight Data

Experimental and predicted longitudinal aerodynamic characteristics are compared with limited flight data from the second flight of the Pegasus vehicle. To lessen the impact on the payload capacity during this

operational flight, only a limited amount of additional instrumentation was carried on board. Details of the flight test and data reduction techniques are found in References 18 and 19. Because of propellent loss due to the burning rocket motor, the center of gravity moves forward during flight. In this paper, the flight pitching moment coefficient data are referenced to the center of gravity position at a given point in time, or the instantaneous center of gravity.

Results and Discussion

Pegasus and Pegasus XL Aerodynamics

Longitudinal aerodynamic characteristics of the Pegasus and Pegasus XL configurations are shown in Figures 7 and 8. At all Mach numbers, aerodynamic performance and longitudinal stability of the two configurations are similar, with the Pegasus XL having slightly more lift and nose-down pitching moment at higher angles of attack. At the lower Mach numbers, the lift curve remains nearly linear through an angle of attack of 24 degrees. At higher Mach numbers, the effect of vortices shedding off the forebody and wing root occurs at lower angles of attack and the lift curve becomes non-linear. Overall, the lift-curve slope decreases by over a factor of three from a value of approximately 0.06 per degree at a Mach number of 1.6 to 0.015 per degree at a Mach number of 6. While increasing Mach number decreases C_{D_0} by 28 percent, the large loss of lift results in a 38 percent reduction in $(L/D)_{max}$ from 2.7 at Mach 1.6 to 1.65 at M = 6. However, for both configurations $(L/D)_{max}$ occurs at an angle of attack of approximately 12 degrees throughout the Mach number range. Both configurations are longitudinally stable, with negligible values of C_{m_0} at all Mach numbers. Stability levels decrease with increasing Mach number, tending toward neutral stability as the center of pressure moves forward. At the lower Mach numbers, a distinct "break" in the pitching moment curve is evident around an angle of attack of 8–10 degrees. This decrease in stability occurs when a combination of increasing forebody vortex strength and downwash interference on the horizontal tails causes a forward shift in the center of pressure. These vortices may be observed in flow visualization photographs in Figure 9.

Lateral-directional aerodynamic characteristics of the Pegasus and Pegasus XL configurations are presented in Figure 10. At the lower Mach numbers, both configurations show positive directional stability at low angles of attack, becoming increasingly unstable as angle of attack increases and the vertical tail is shadowed by the wing and fuselage. The increased stability of the Pegasus XL configuration at low angles of attack is a result of the effective increase in vertical area due to the horizontal tail anhedral. The directional stability of both configurations tends toward neutral values with increasing Mach number. In addition, the reduced vertical stabilizer effectiveness at higher Mach numbers results in directional instability at low angles of attack and less change in stability levels with angle of attack. Dihedral effect is positive at all conditions, with stability generally decreasing with increasing Mach number. At the lower Mach numbers, dihedral effect decreases at higher angles of attack as flow separates from the upper surface of the wing. This trend diminishes at higher Mach numbers where the windward flow supports a greater percentage of the lift. The anhedral of the horizontal stabilizers on the Pegasus XL results in a 30–50 percent reduction in roll stability due to the projected side area of the tails below the center of gravity.

Control effectiveness for both configurations is shown in Figures 11 and 12 for a Mach number of 2.0. Elevon effectiveness is noticeably greater for the Pegasus XL configuration at all angles of attack due to the longer moment arm and tail anhedral angle which reduces fuselage interference and places the surfaces further from the wing downwash. Pitch effectiveness for the Pegasus XL increases by 50 percent with angle of attack and, at high angles of attack, is 37 percent higher than for the Pegasus configuration. Aileron (differential tail deflection) and rudder roll effectiveness vary little between the two configurations and are nearly constant with angle of attack. There is a noticeable effect of aileron deflection on yawing moment for the Pegasus XL due to the side force component produced when the anhedral tails are deflected. For both configurations, $C_{n_{\delta_a}}$ increases with angle of attack as the lift, and hence the drag due to lift, decreases on the downward-deflected (port) horizontal stabilizer and increases on the upward-deflected (starboard) stabilizer. The difference in drag between the port and starboard tails results in a positive yawing moment increment. Rudder effectiveness is greater for the Pegasus XL due to the longer moment arm of the vertical tail. The rudder effectiveness for both configurations, and the difference in effectiveness between the two, decrease with angle of attack as the vertical tail becomes shadowed by the fuselage.

Comparison of Experiment and Prediction

Comparisons of the experimental data with APAS predictions based on wind tunnel flow conditions and NEAR predictions for flight conditions are presented in Figures 13 through 17 for the Pegasus configuration. Since the predictions and experiment were not all conducted at the same Mach numbers, comparisons are generally presented only for cases where the Mach numbers are identical. However, at the high end of the Mach number range, experimental data at Mach 6 are com-

pared with NEAR predictions at a Mach number of 5.0.

Experimental and predicted longitudinal aerodynamic characteristics of the Pegasus configuration are shown in Figures 13 and 14. As compared to the experimental results, the NEAR data base generally gives a better overall prediction of the longitudinal aerodynamics than the APAS code. Lift-curve slope is overpredicted by APAS due to the inability of the code to handle separated flow regions. The prediction improves at higher Mach numbers where the leeside flow has less contribution to the overall lift. Lift-curve slope data from the NEAR codes, which employ empirical databases and leeside vortex models, compare well with the experimental data throughout the Mach number range. At low Mach numbers, both codes predict less longitudinal stability than the experimental results. The comparison improves with Mach number as lift becomes dominated by the windward flow and the codes are better able to predict the overall pressure distribution and hence the location of the center of pressure. The NEAR results give a better prediction of drag coefficient and lift-to-drag ratio, particularly at high angles of attack where APAS overpredicts lift. Zero-lift drag coefficient results from the APAS code compare well with experimental data except at lower Mach numbers, where APAS predicts a 26 percent higher value of C_{D_0}. At Mach numbers above 1.6, the NEAR predictions yield values of C_{D_0} up to 15 percent higher than experiment. This is a result of the attempt by NEAR to factor in increased drag due to protuberances and surface roughness on the flight vehicle that are not modelled in the wind tunnel.

The flowfield about the Pegasus vehicle is quite complex, particularly at sideslip, with large areas of flow separation and vortices above and below the wing. (See again Figure 9.) Consequently, the predicted lateral-directional aerodynamic characteristics do not compare as favorably with the experimental data, as is evident in Figure 15. Over the Mach number range, the NEAR results generally provide a better prediction of directional stability than APAS. Because APAS does not model separated flow regions, the wake flow over the vertical tail and subsequent loss of directional stability at high angles of attack are not predicted. Rather, the APAS results show positive directional stability through the angle of attack range, tending toward neutral stability with increasing Mach number. At lower Mach numbers, directional stability predictions from NEAR compare well with experimental results through an angle of attack range of 12 degrees. At higher angles, the predictions show less directional instability than the experimental data. The comparison is not as favorable at higher Mach numbers, where the NEAR codes predict higher levels of directional instability. The APAS code yields a better prediction of side force and the general level of dihedral effect, although neither prediction models the reduction in roll stability at high angles of attack that results from flow separation on the wing.

Comparisons of control effectiveness from prediction and experimental data are shown in Figures 16 and 17. Longitudinal control effectiveness results from NEAR are in good agreement with experiment, except at Mach 6, where both the NEAR and APAS predictions show twice the lift and pitching moment effectiveness. This discrepancy is unexpected considering the good agreement at lower Mach numbers, and no plausible expanation can be given at this time. Across the Mach number range (except for Mach 6), APAS overpredicts elevon effectiveness at low to moderate angles of attack by about 12 and 28 percent, respectively, for lift and pitching moment. Results from the NEAR predictions for rolling moment due to both aileron and rudder deflection compare well with experimental data in all cases. Similar results from APAS show 25 percent greater effectiveness at low supersonic Mach numbers, with improving agreement at higher Mach numbers. Rudder effectiveness is generally not as well predicted. APAS compares well at a Mach number of 1.6, but shows increasingly less effectiveness than experiment, up to 30 percent, as Mach number increases to 2.96. Agreement at Mach 6 is excellent. Data from NEAR show a reduction in rudder effectiveness at angles of attack above 12 degrees for most of the Mach number range. This decrease, as much as 36 percent at a Mach number of 2.0, is not borne out by experimental results.

Comparisons of Experimental and Flight Data

In the comparison of experimental and flight data, the flight data were used as the baseline condition. Experimental data were interpolated to the flight angle of attack and corrected for elevon deflection before being referenced to the instantaneous center of gravity. Flight angle of attack and elevon deflection histories are shown in Figure 18, and comparisons of the longitudinal data are presented in Figure 19. The agreement between experiment and flight measured values of lift coefficient is very good across the Mach number range. Wind tunnel data capture the trend in drag coefficient but are approximately 15 percent lower than flight values. These lower drag coefficient numbers account for the increased values of lift-to-drag ratio at the lower Mach numbers. The higher drag coefficient values for flight may be the result of protuberances on the flight vehicle (antennae, hatches, etc) which are not represented on the wind tunnel model, and also increased skin friction due to the surface roughness of the thermal protection system. Flight and experimental pitching moment data for a trimmed configuration are in excellent agreement except at the lower Mach numbers. At a Mach number of 1.6, the dif-

ference in pitching moment coefficient is equivalent to a forward shift in center of gravity or rearward shift in center of pressure of 0.59 feet, or 1.2 percent of the body length. This discrepancy is not unexpected given the complex nature of the flowfield at high angles of attack.

Concluding Remarks

Experimental longitudinal and lateral-directional aerodynamic characteristics for the Pegasus and Pegasus XL configurations were obtained for a range of Mach number from 1.6 to 6 and angles of attack from -4 degrees to 24 degrees. Experimental data for the Pegasus configuration are compared with those for the Pegasus XL configuration; with predictions from NEAR and the APAS code; and with flight data. Longitudinal, lateral-directional, and control effectiveness data are presented.

Results indicate that the longitudinal aerodynamic characteristics for the Pegasus and Pegasus XL configurations are very similar. Both vehicles are longitudinally stable over the angle of attack range, with a trend toward neutral stability at higher Mach numbers as the center of pressure moves forward. At moderate to high angles of attack, both configurations become directionally unstable as the vertical tail becomes shadowed by the fuselage and wing. Dihedral effect is positive at all Mach numbers, tending toward neutral values at high angles of attack. The anhedral on the horizontal tails of the Pegasus XL reduce the roll stability by 30–50 percent. Longitudinal and lateral-directional control effectiveness decrease with increasing Mach number. The Pegasus XL shows slightly greater elevon effectiveness and a aileron yawing moment increment due to the horizontal tail anhedral.

Predictions from NEAR and the APAS code yield good assessments of longitudinal aerodynamics and both longitudinal and lateral-directional control effectiveness. Due to the inability to model separated flow, the APAS code overpredicts the lift-curve slope at lower Mach numbers. Calculations for lateral-directional aerodynamic characteristics were not in good agreement with experiment. Predictions from NEAR overestimate directional stability at higher Mach numbers and underestimate roll stability and side force at most conditions. Except at high Mach numbers, the APAS code yields poor predictions of directional stability. Estimations of side force and dihedral effect, however, are generally better than those from NEAR for the Pegasus configuration.

Experimental longitudinal aerodynamic data compare fairly well with flight data across the Mach number range. Experimentally-measured values of drag coefficient are approximately 15 percent lower than flight values. At low supersonic Mach numbers, experimental results for a trimmed flight condition show a slight negative pitching moment, equivalent to a rearward shift in center of pressure of 1.2 percent of the body length.

A better understanding of the capabilities of preliminary aerodynamic analysis tools will improve the efficiency and accuracy of such analyses in the design cycle of future air-launched SPOVs. Current prediction methodologies such as those used in the design of the Pegasus vehicle provide reasonably good assessments of longitudinal aerodynamic and control effectiveness characteristics; however, for configurations with complex, vortex-dominated flowfields, wind tunnel studies are required to provide credible lateral-directional aerodynamic characteristics.

Acknowledgments

The author would like to thank Mr. Robert Curry of NASA Dryden Flight Research Center and Mr. Bryan Moulton of PRC, Inc., Edwards, California, who provided the flight data presented in this paper.

References

1. Asker, J. R.: "Racing to Remake Space Economics." *Aviation Week & Space Technology,* April 3, 1995.

2. Schade, C: "Pegasus, Taurus, and Glimpses of the Future." AIAA Paper 90-3573, September 1990.

3. Meyer, R. R., Jr.; Curry, R. E.; and Budd, G. D.: "Aerodynamic Flight Research Using the Pegasus Air-Launched Booster." AIAA Paper 92-3990, July 1992.

4. Bertelrud, A.; Kolodziej, P.; Noffz, G. K.; and Godil, A.: "Plans for In-Flight Measurement of Hypersonic Crossflow Transition of the Pegasus Launch Vehicle." AIAA Paper 92-4104, August 1994.

5. "X-34 to be Acid Test for Space Commerce." *Aviation Week & Space Technology,* April 3, 1995.

6. Mendenhall, M. R.; Lesieutre, D. J.; Caruso, S. C.; Dillenius, M. F. E.; and Kuhn, G. D.: "Aerodynamic Design of Pegasus — Concept to Flight with CFD." AGARD Symposium on Missile Aerodynamics, Friedrichshafen, Germany, April 1990.

7. Mendenhall, M. R.; Lesieutre, D. J.; Whittaker, C. H.; Curry, R. E.; and Moulton, B.: "Aerodynamic Analysis of Pegasus — Computations vs Reality." AIAA Paper 93-0520, January 1993.

8. Jackson, C. M., Jr.; Corlett, W. A.; and Monta, W. J.: *Description and Calibration of the Langley Unitary*

Plan Wind Tunnel. NASA TP 1905, 1981.

9. Miller, C. G.: "Langley Hypersonic Aerodynamic/Aerothermodynamic Testing Capabilities—Present and Future." AIAA Paper 90–1376, June 1990.

10. Braslow, A. L.; Hicks, R. M.; and Harris, R. V., Jr.: *Use of Grit-Type Boundary Layer Transition Trips on Wind Tunnel Models.* NASA TN D-3579, 1966.

11. Kline, S. J. and McClintock, F. A.: "Describing Uncertainties in Single- Sample Experiments." *Mechanical Engineering*, Vol. 75, No. 1, pp 3-9, January 1953.

12. Coleman, H. W. and Steele, W. G., Jr.: *Experimentation and Uncertainty Analysis for Engineers,* John Wiley & Sons, 1989.

13. Bathill, S. P.: *Experimental Uncertainty and Drag Measurements in the National Transonic Facility,* NASA CR 4600, 1994.

14. Tripp, J. and Tcheng, P.: "Determination of Measurement Uncertainty of Multi-Component Wind Tunnel Balances." AIAA Paper 94-2589, June 1994.

15. Cruz, C. I. and Wilhite, A. W.: "Prediction of High-Speed Aerodynamic Characteristics Using the Aerodynamic Preliminary Analysis System (APAS)." AIAA Paper 89-2173, July 1989.

16. Engelund, W. C. and Ware, G. M.: "Aerodynamic Predictions and Experimental Results for an Advanced Manned Launch System Orbiter Configuration." AIAA Paper 93-1020, February 1993.

17. Gentry, A: *Hypersonic Arbitrary-Body Aerodynamic Computer Program (Mark III Version), Vol. II: Program Formulation and Listings.* Douglas Report DAC 61552, April 1968.

18. Curry, R. E.; Mendenhall, M. R.; and Moulton, B.: *In-Flight Evaluation of Aerodynammic Predictions of an Air-Launched Space Booster.* NASA TM 104246, 1992.

19. Noffz, G. K.; Curry, R. E.; Haering, E. A., Jr.; and Kolodziej, P.: *Aerothermal Test Results From the First Flight of the Pegasus Air-Launched Space Booster.* NASA TM 4330, 1991.

Table 1. Model geometric characteristics. (all dimensions in inches or inches^2).

Dimension	Pegasus	Pegasus XL
Model length, L	17.774	19.974
Wing span, b	7.920	7.920
Reference length, $\bar{c}$	2.934	2.934
Reference area, S	18.912	18.912
Wing aspect ratio, AR	3.333	3.333
Wing taper ratio, λ	0.092	0.092
Wing leading edge sweep, Λ_{LE}	45°	45°
Horizontal tail dihedral angle, Γ_{tail}	0°	-23°

Table 2. Flow conditions.

Facility	M_∞	P_t, psia	T_t, °R	P_∞,psia	T_∞,°R	q_∞,psia	Re x 10^{-6}/ft
UPWT	1.60	7.49	585	1.762	387	3.16	2.0
UPWT	2.00	8.70	585	1.113	325	3.11	2.0
UPWT	2.50	11.1	585	0.650	260	2.85	2.0
UPWT	2.96	14.2	585	0.409	213	2.51	2.0
UPWT	3.95	25.1	610	0.177	148	1.93	2.0
UPWT	4.63	34.3	610	0.101	115	1.52	2.0
20-Inch Mach 6 Tunnel	5.92	60	885	0.042	110	1.03	1.0
20-Inch Mach 6 Tunnel	5.98	125	910	0.083	112	2.05	2.0
20-Inch Mach 6 Tunnel	6.00	195	935	0.124	114	3.13	3.0

Table 3. Uncertainties in body-axis aerodynamic coefficients.

	Mach Number						
	1.60	2.00	2.50	2.96	3.95	4.63	5.98
ΔC_N	.0064	.0052	.0043	.0038	.0032	.0033	.0021
ΔC_A	.0005	.0005	.0006	.0007	.0009	.0011	.0008
ΔC_m	.0036	.0027	.0021	.0020	.0017	.0022	.0004
ΔC_l	.0004	.0003	.0003	.0003	.0003	.0004	.0002
ΔC_n	.0014	.0012	.0006	.0004	.0005	.0006	.0002
ΔC_Y	.0026	.0025	.0024	.0026	.0026	.0028	.0018

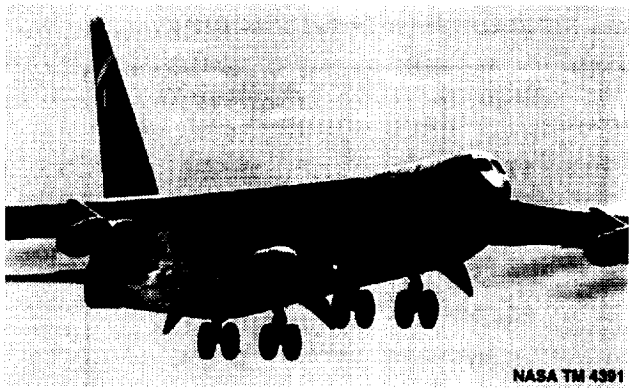

Figure 1. Pegasus vehicle on B-52 carrier aircraft.

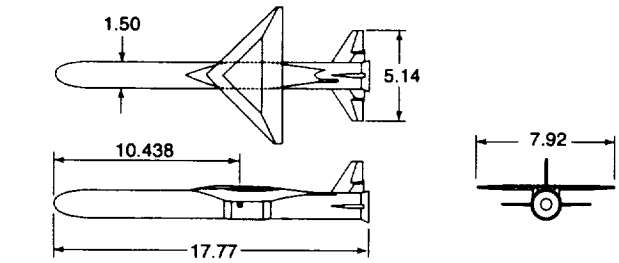

(a) Pegasus

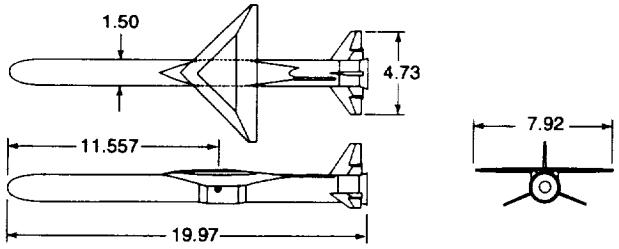

(b) Pegasus XL

Figure 2. Sketches of Pegasus and Pegasus XL models. All dimensions are given in inches.

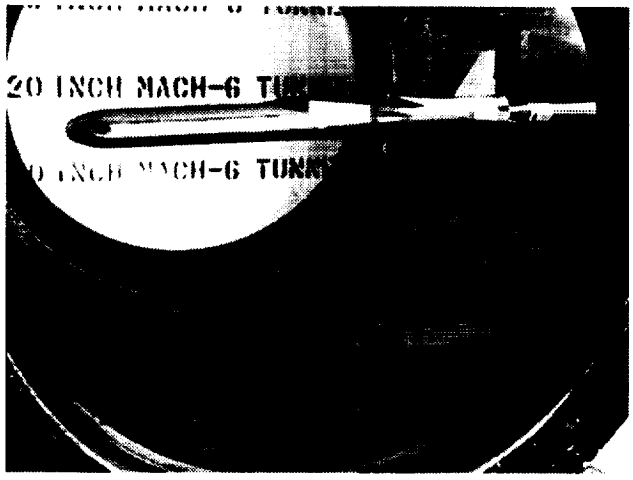

Figure 3. Photograph of Pegasus model in 20-Inch Mach 6 Tunnel.

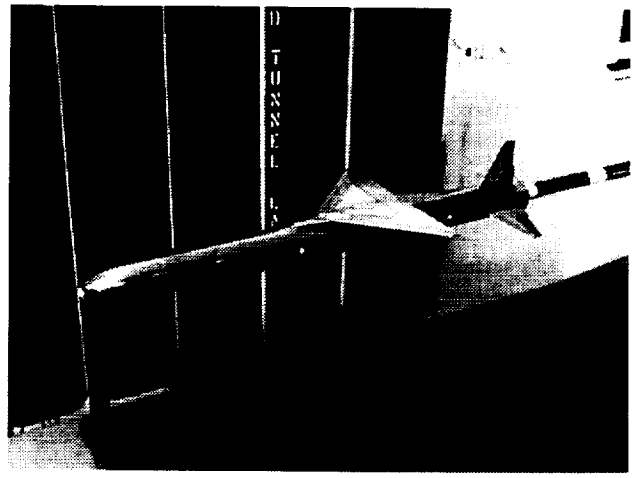

Figure 4. Photograph of Pegasus XL model in UPWT.

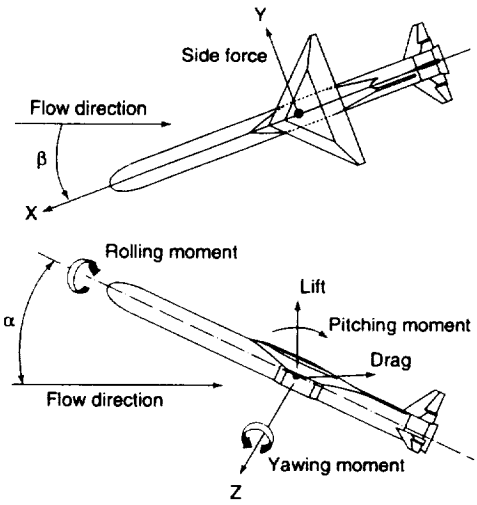

Figure 5. Coordinate system.

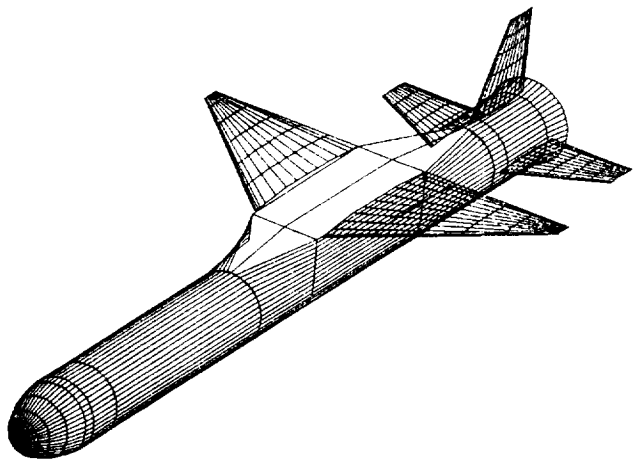

Figure 6. Pegasus paneled-body model used in APAS predictions.

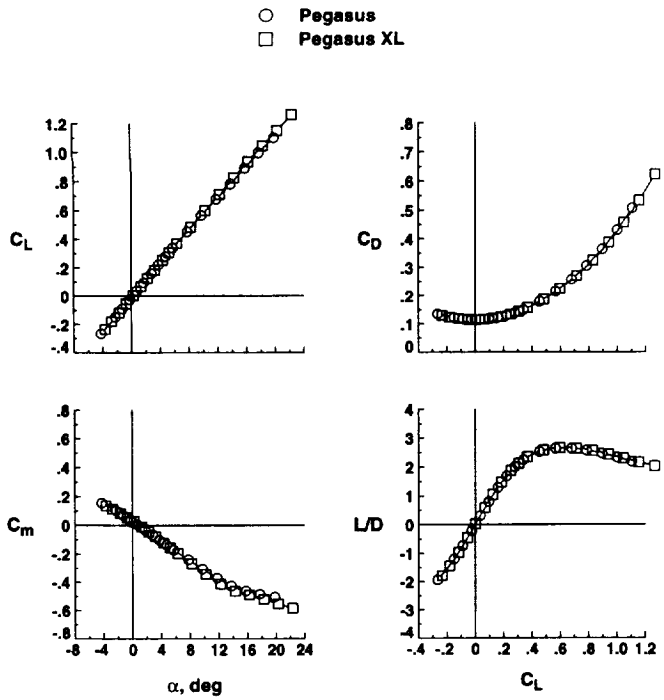

(a) $M_\infty = 1.6$

Figure 7. Longitudinal aerodynamic characteristics of Pegasus and Pegasus XL configurations.

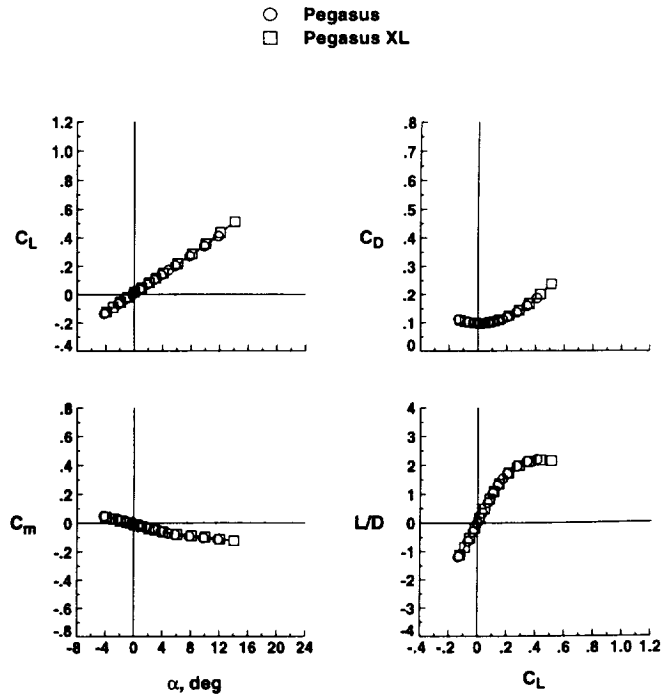

(c) $M_\infty = 2.96$

Figure 7. Continued.

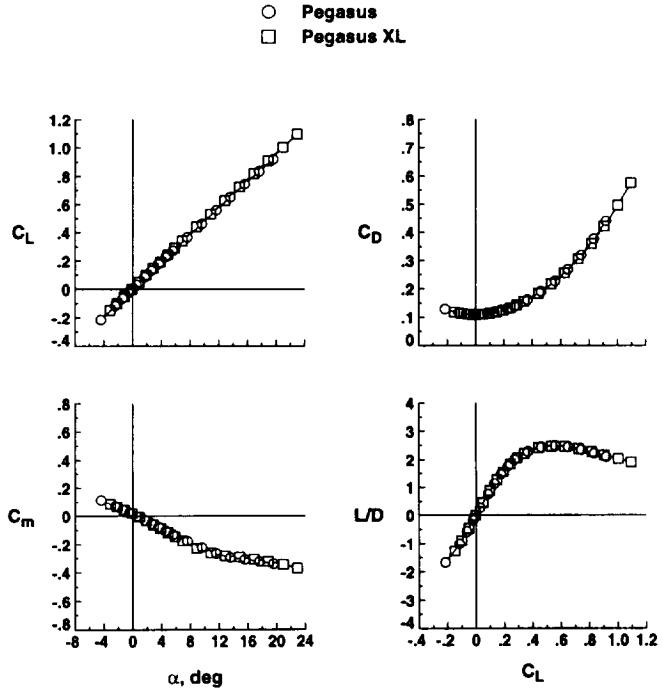

(b) $M_\infty = 2.0$

Figure 7. Continued.

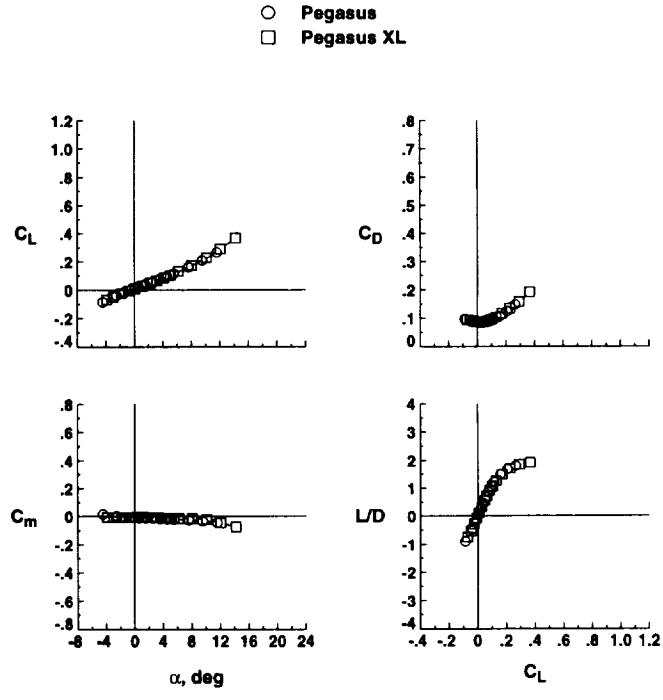

(d) $M_\infty = 4.63$

Figure 7. Continued.

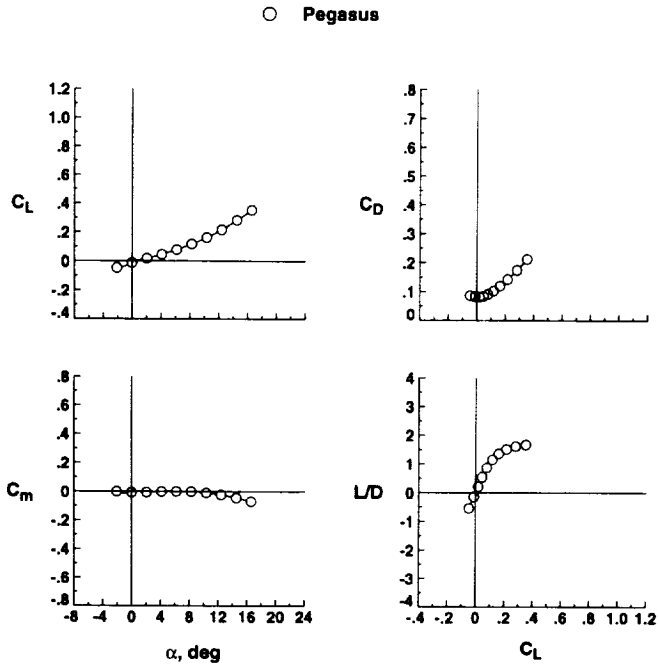

(e) $M_\infty = 6.0$

Figure 7. Concluded.

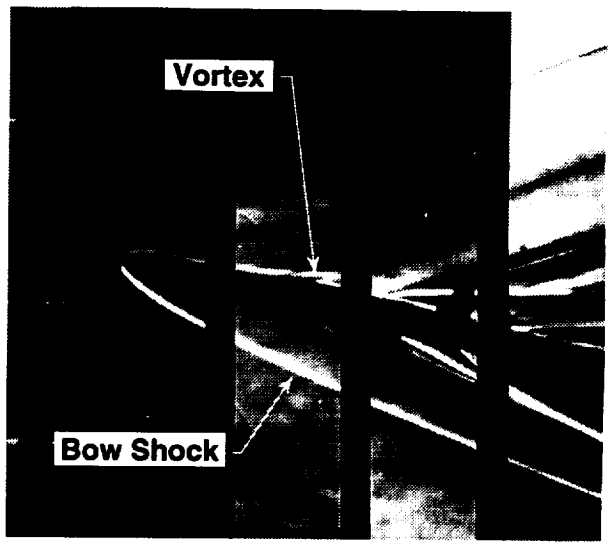

(a) Schlieren

Figure 9. Flow visualization results at $M_\infty = 2.5$ and $\alpha = 12°$.

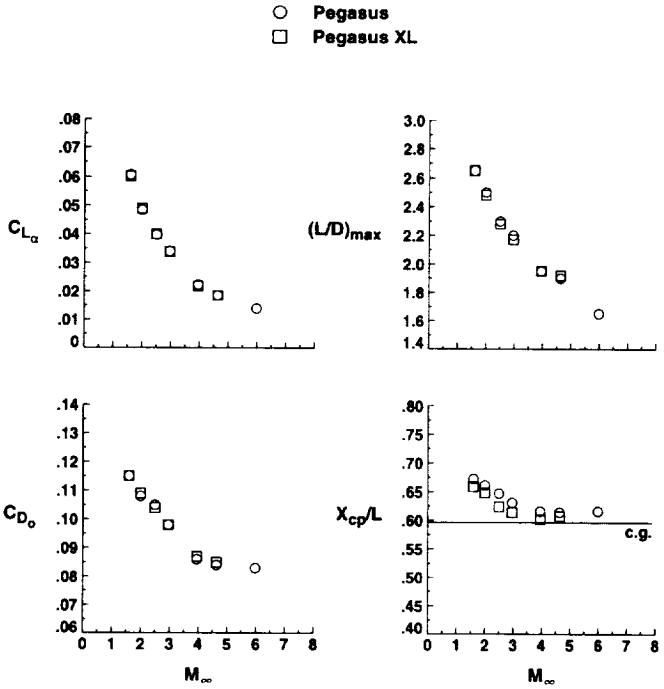

Figure 8. Summary of longitudinal aerodynamic characteristics of Pegasus and Pegasus XL configurations.

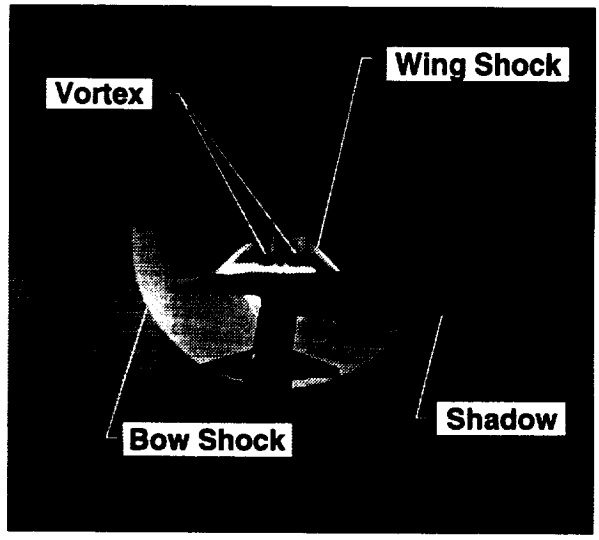

(b) Vapor screen

Figure 9. Concluded.

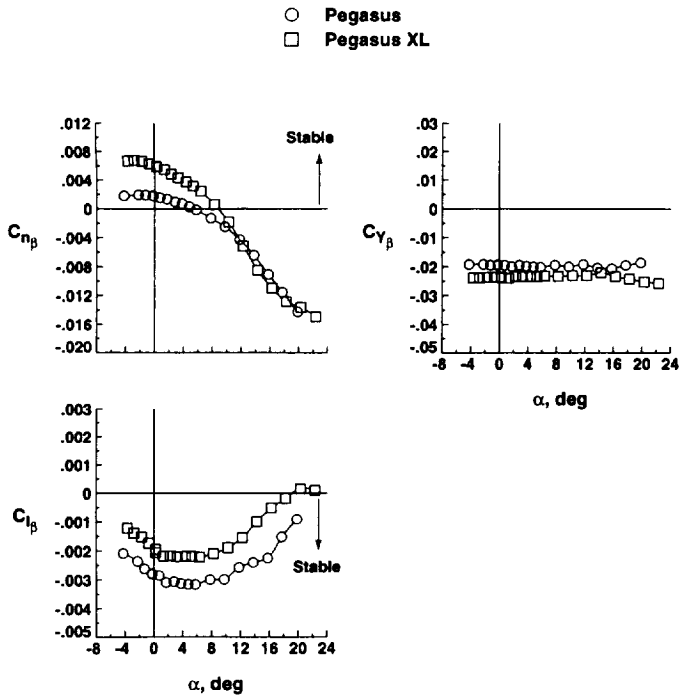

(a) $M_\infty = 1.6$

Figure 10. Lateral-directional aerodynamic characteristics of Pegasus and Pegasus XL configurations.

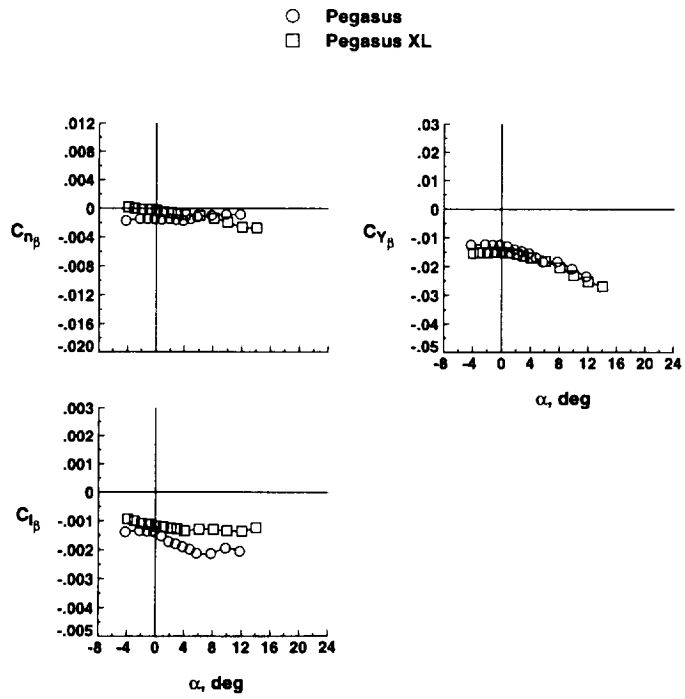

(c) $M_\infty = 2.96$

Figure 10. Continued.

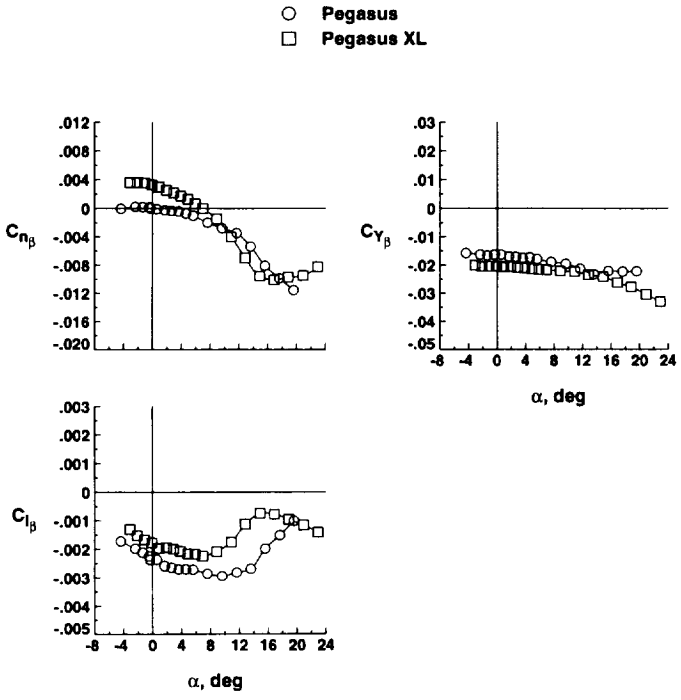

(b) $M_\infty = 2.0$

Figure 10. Continued.

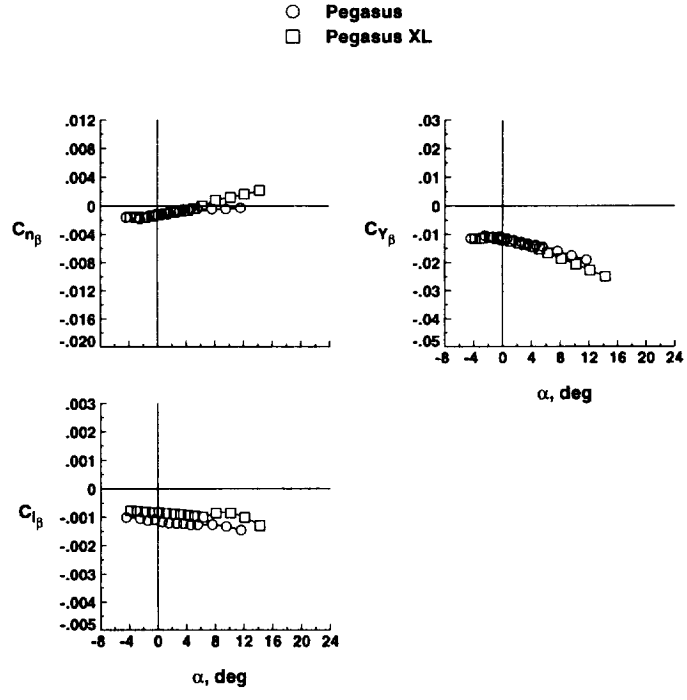

(d) $M_\infty = 4.63$

Figure 10. Continued.

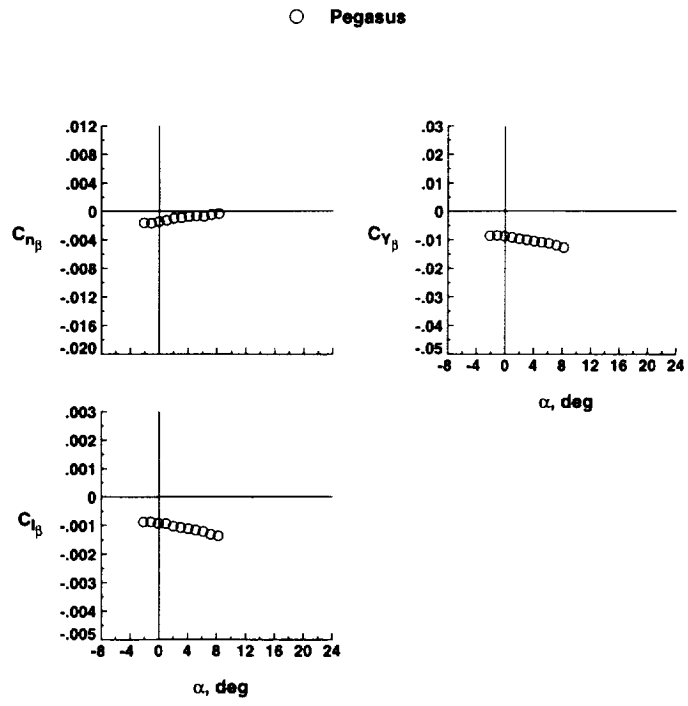

(e) $M_\infty = 6.0$

Figure 10. Concluded.

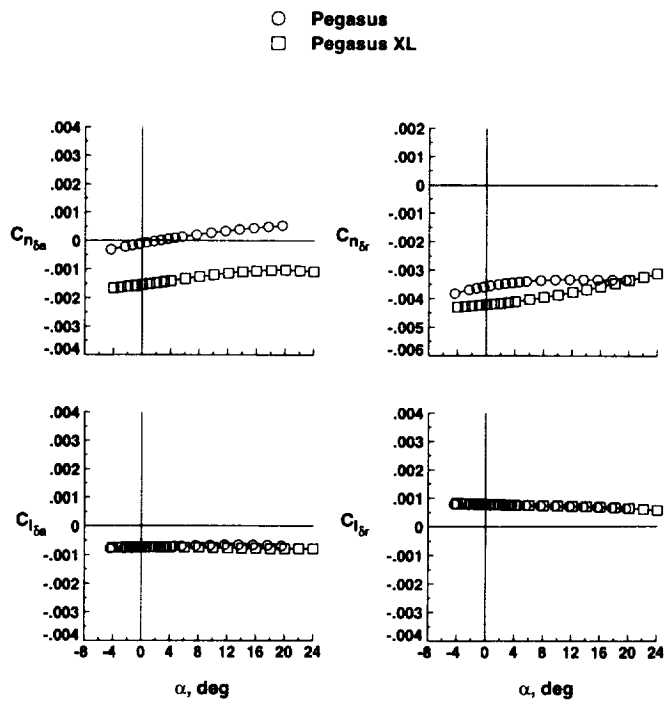

Figure 12. Lateral-directional control effectivness for Pegasus and Pegasus XL configurations at $M_\infty = 2.0$.

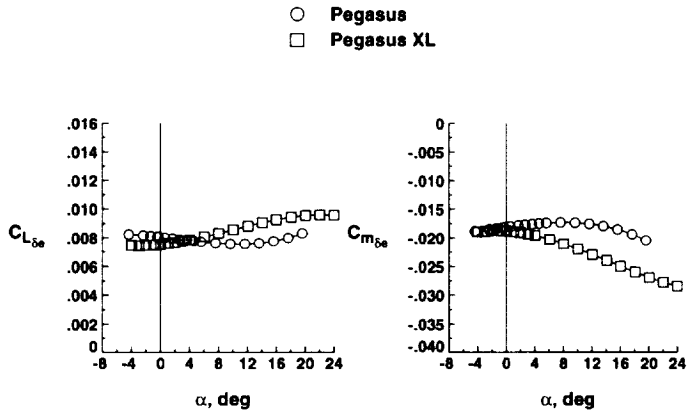

Figure 11. Longitudinal control effectiveness for Pegasus and Pegasus XL configurations at $M_\infty = 2.0$.

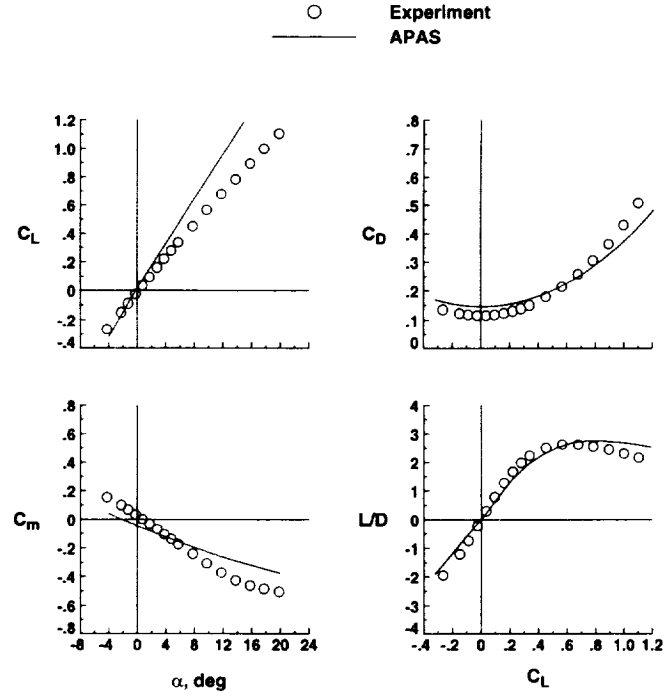

(a) $M_\infty = 1.6$

Figure 13. Comparison of experimental and predicted longitudinal aerodynamic characteristics for Pegasus configuration.

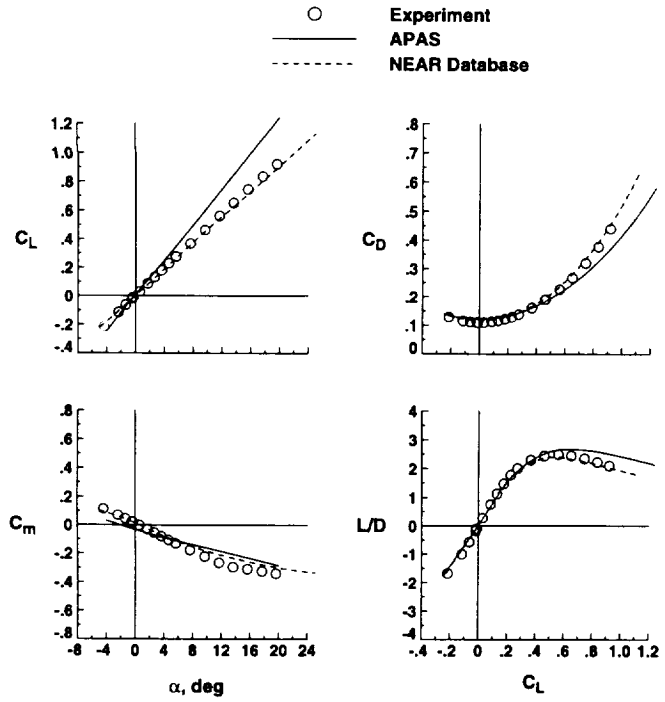

(b) $M_\infty = 2.0$

Figure 13. Continued.

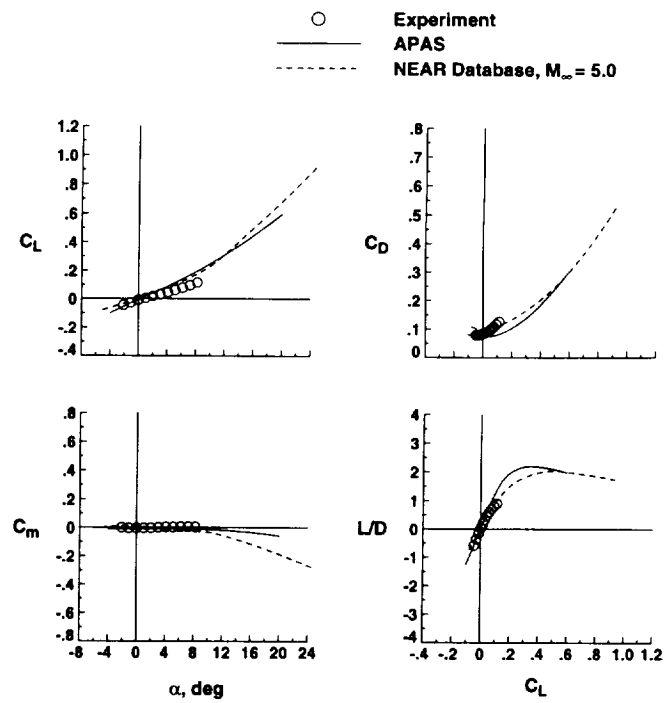

(d) $M_\infty = 6.0$

Figure 13. Concluded.

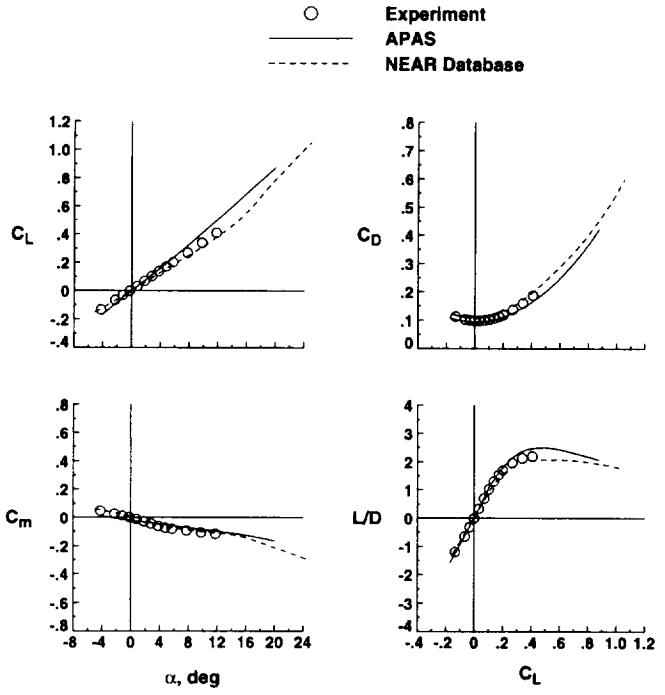

(c) $M_\infty = 2.96$

Figure 13. Continued.

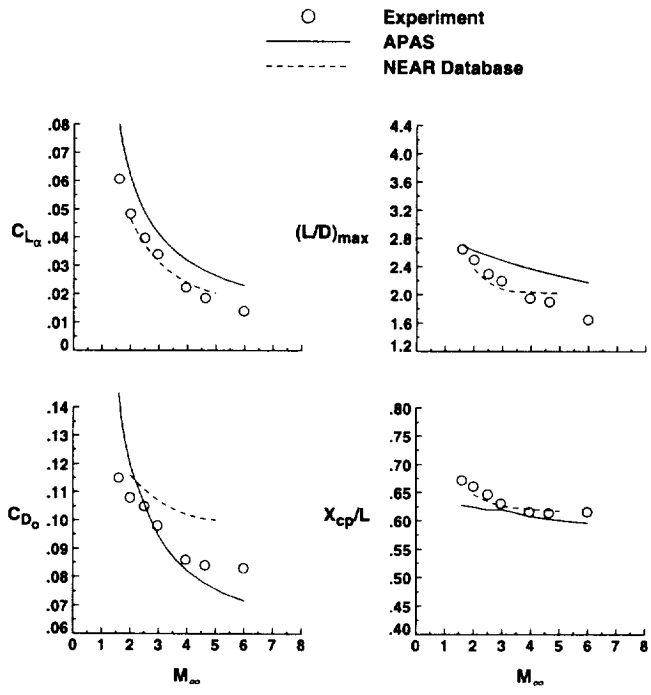

Figure 14. Summary of experimental and predicted longitudinal aerodynamic characteristics for Pegasus configuration.

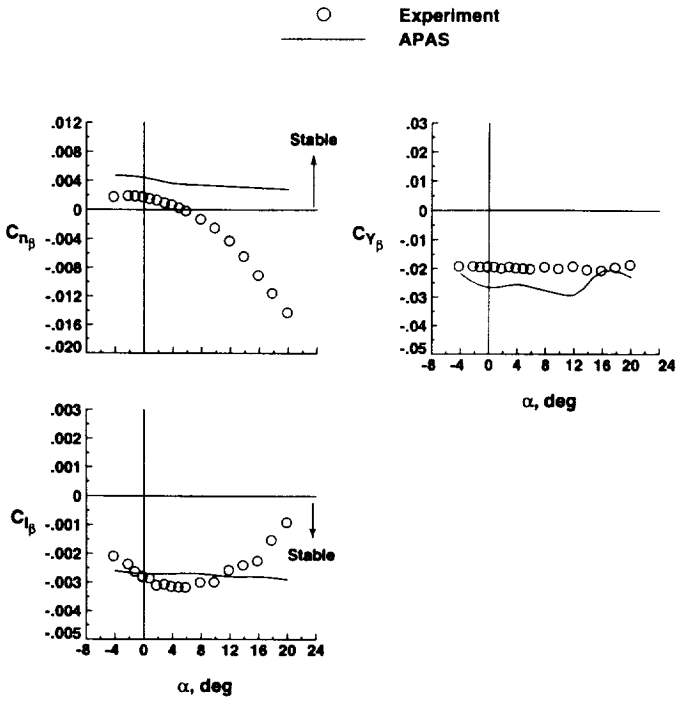

(a) $M_\infty = 1.6$

Figure 15. Comparison of experimental and predicted lateral-directional aerodynamic characteristics for Pegasus configuration.

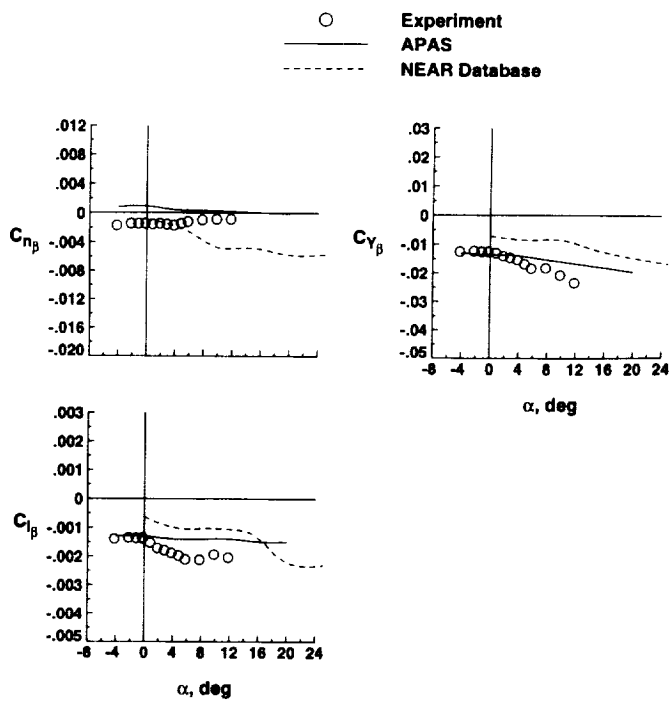

(c) $M_\infty = 2.96$

Figure 15. Continued.

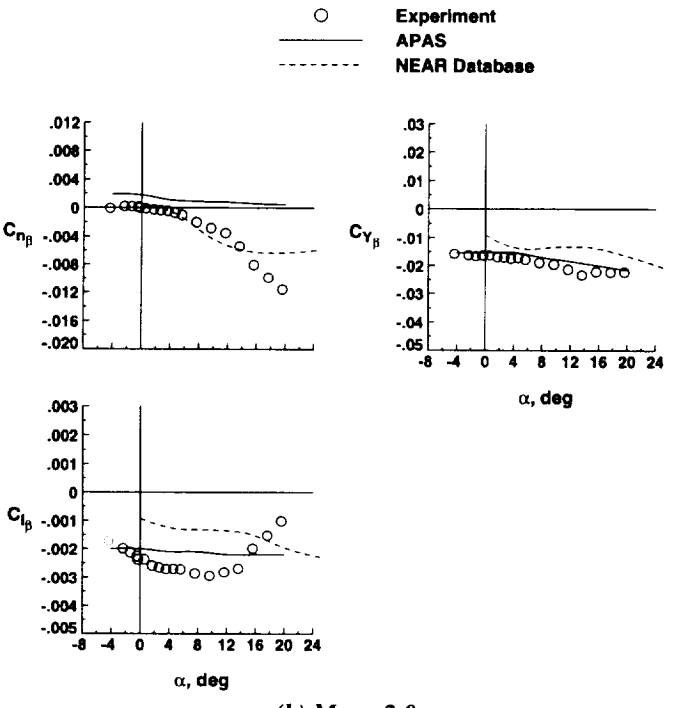

(b) $M_\infty = 2.0$

Figure 15. Continued.

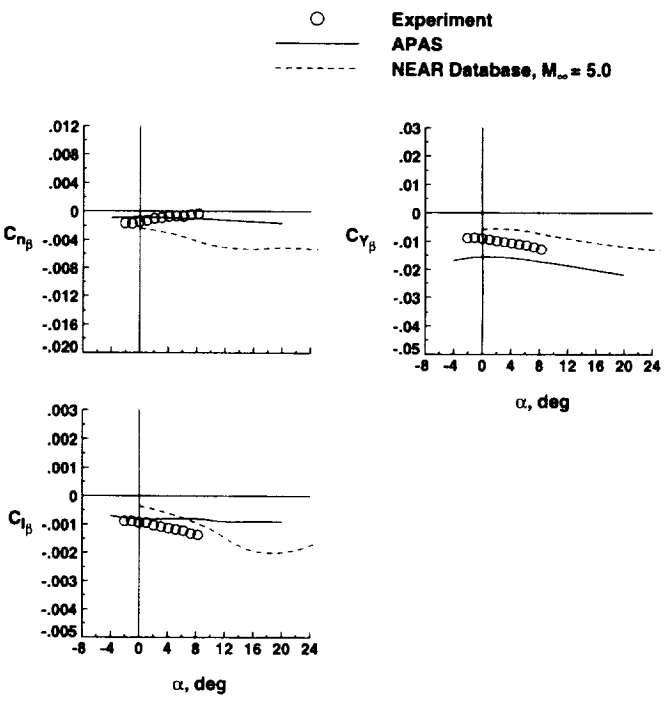

(d) $M_\infty = 6.0$

Figure 15. Concluded.

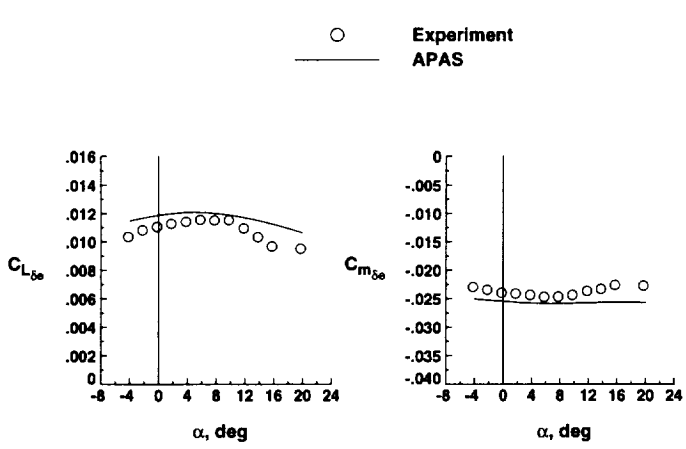

(a) $M_\infty = 1.6$

Figure 16. Comparison of experimental and predicted longitudinal control effectiveness for Pegasus configuration.

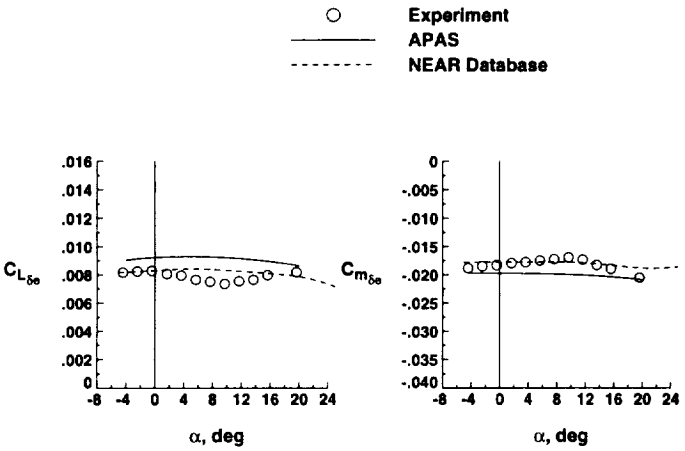

(b) $M_\infty = 2.0$

Figure 16. Continued.

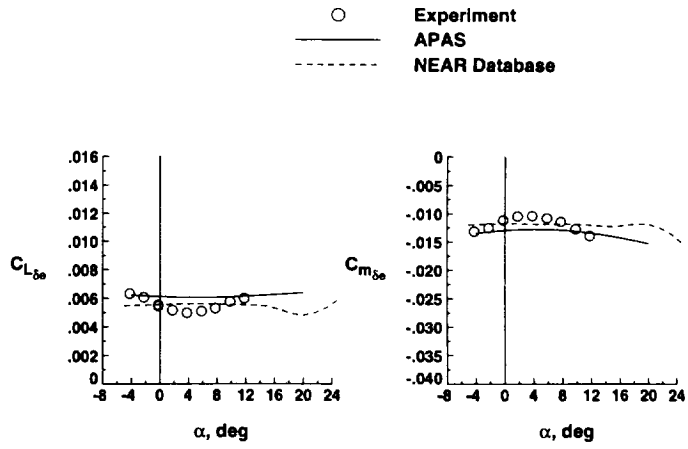

(c) $M_\infty = 2.96$

Figure 16. Continued.

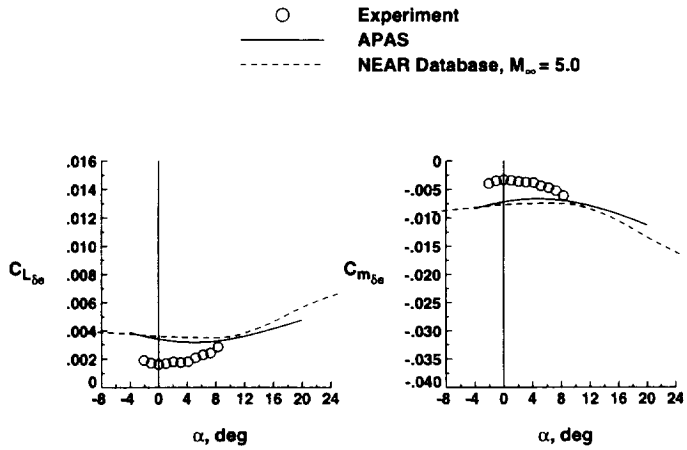

(d) $M_\infty = 6.0$

Figure 16. Concluded.

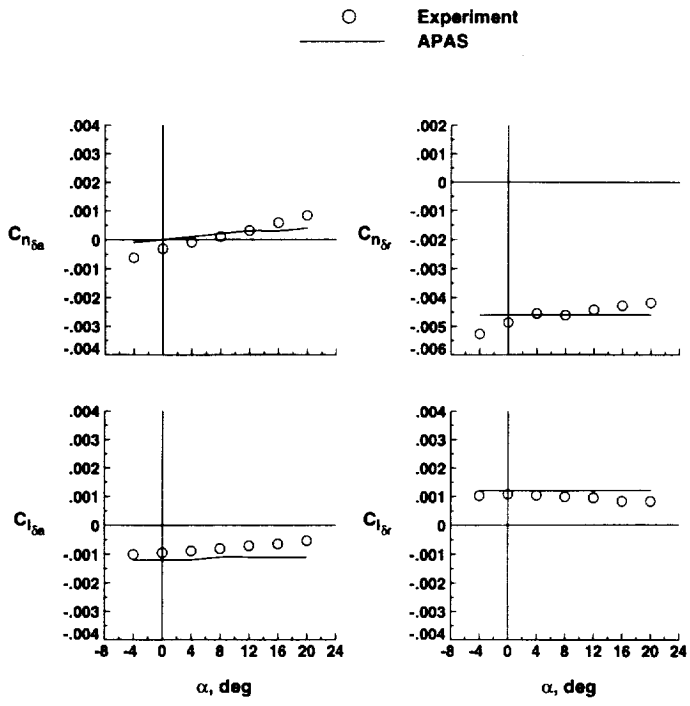

(a) $M_\infty = 1.6$

Figure 17. Comparison of experimental and predicted lateral-directional control effectiveness for Pegasus configuration.

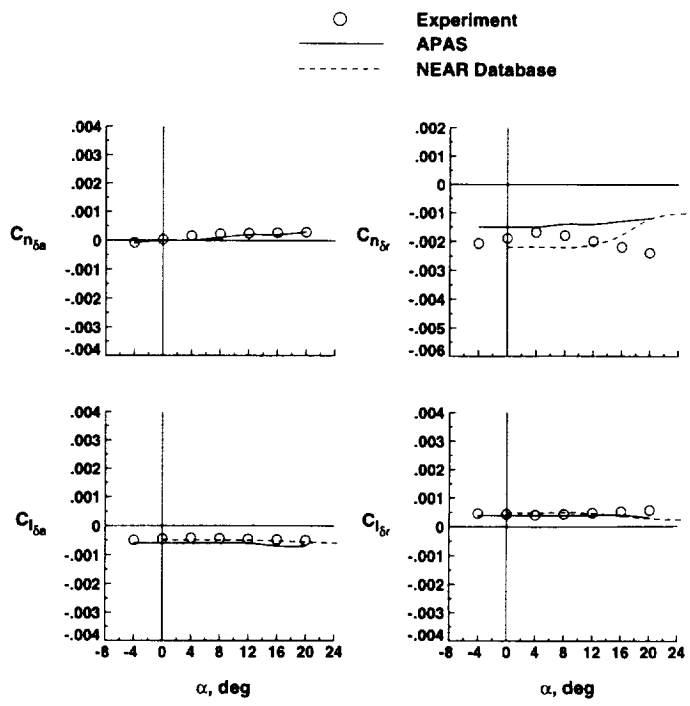

(c) $M_\infty = 2.96$

Figure 17. Continued.

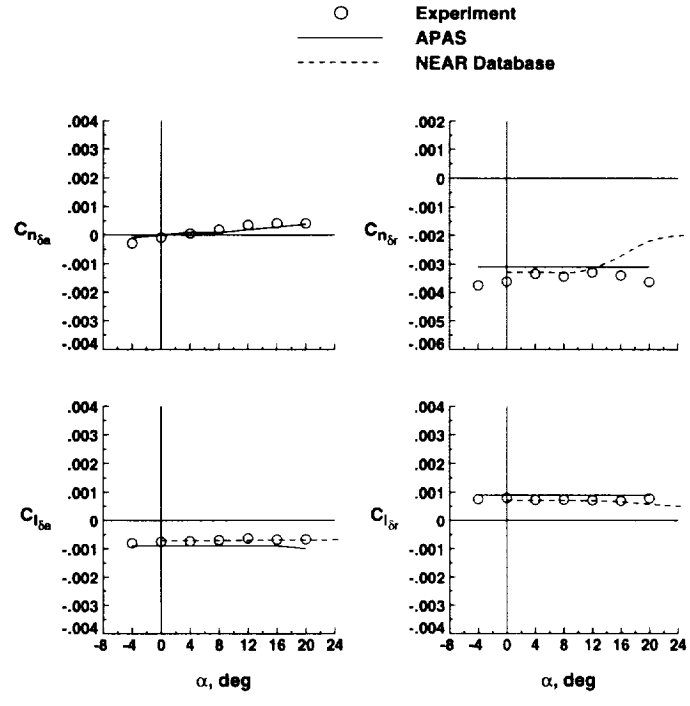

(b) $M_\infty = 2.0$

Figure 17. Continued.

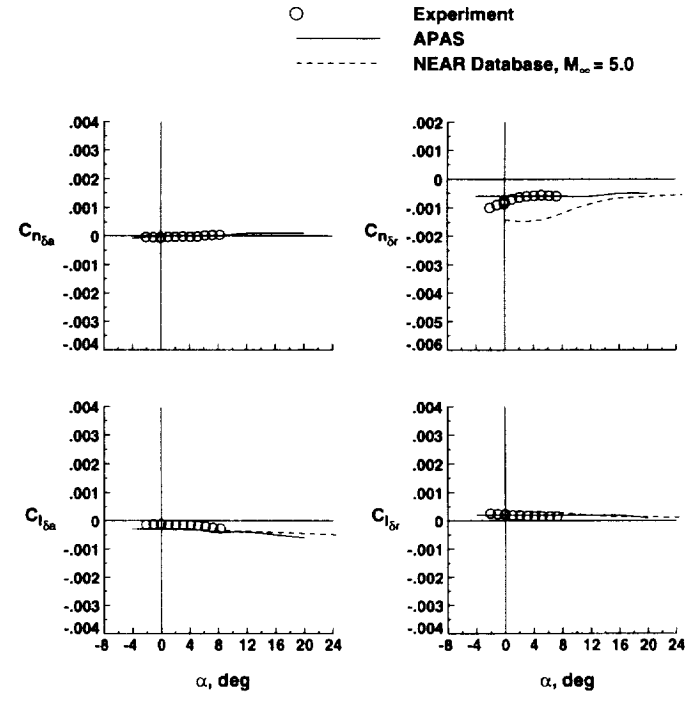

(d) $M_\infty = 6.0$

Figure 17. Concluded.

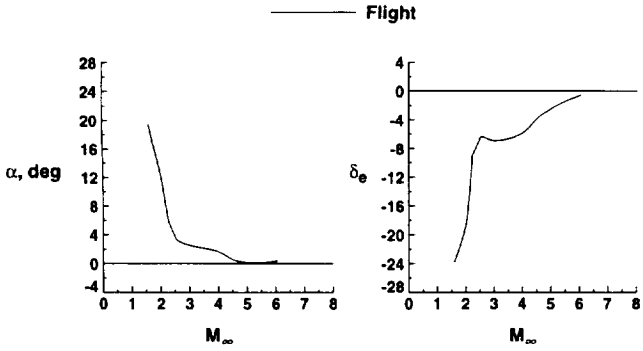

Figure 18. Angle of attack and elevon deflection histories for Pegasus Flight #2.

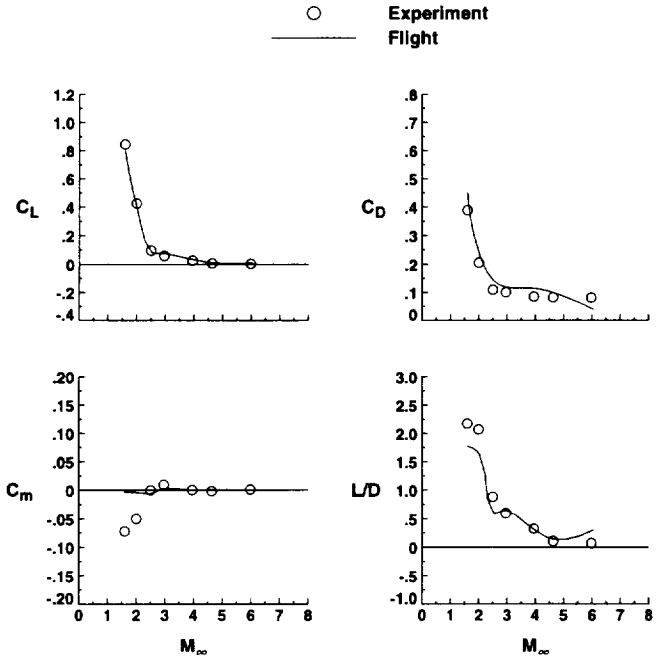

Figure 19. Comparison of experimental and flight longitudinal aerodynamic data for Flight #2 of the Pegasus vehicle.